ELSEVIER

Surface Science 460 (2000) 12–20

surface science

www.elsevier.nl/locate/susc

Scattering of N_2 from Ni(111)

Carl M. Matthews, Frank Balzer, Alexander J. Hallock, Mark D. Ellison [1], Richard N. Zare *

Department of Chemistry, Stanford University, Stanford, CA 94305, USA

Received 21 December 1999; accepted for publication 13 March 2000

Abstract

A cold ($T_{rot} < 10$ K) beam of N_2 with an initial translational energy of 0.40 eV strikes an Ni(111) surface at surface temperatures from 300 to 873 K at several incident angles from 15 to 60°. The rotational energy and angular distributions of the scattered molecules are probed using (2+1) resonance-enhanced multiphoton ionization. Molecules scattered in the specular direction have mean rotational energies that are independent of surface temperature, whereas those scattered at angles far from the specular show a dependence on surface temperature, caused likely by multiple collisions with the surface before escape. A rotational rainbow, seen in systems such as CO–Ni(111) and N_2–Ag(111), is not seen in this system. For molecules that scatter close to the specular direction, approximately 10% of the initial translational energy is converted into rotational energy of the scattered N_2. For surface temperatures above room temperature, the angular distributions indicate that molecules that scatter into low-J states also tend to exit in a broad peak (10–20° FWHM) near the specular, and this peak is broadened with increasing incident angle. The molecules that scatter into high-J states have a much broader distribution, indicating that they are trapped rotationally during the initial collision and suffer multiple collisions before leaving the surface.

Keywords: Energy dissipation; Laser methods; Low index single crystal surfaces; Nickel; Nitrogen molecule; Resonance enhanced multiphoton ionization mass spectroscopy (REMPI/MS)

1. Introduction

Molecular beam scattering experiments have long been used to investigate the details of an interaction potential. This technique has been used with great success to study the interactions of atoms and molecules with solid surfaces [1]. Many standard surface science techniques exist that, when used in a complementary fashion, yield much information about the adsorbed state, but the microscopic dynamics of the adsorption process cannot be determined by such experiments. Instead, the dynamics may be inferred from careful studies of scattered particles. For example, Hines and Zare [2] demonstrated that, at incident kinetic energies near 0.4 eV, CO molecules striking an Ni(111) surface are more likely to scatter if they strike O-end first. Those that strike the surface C-end first have a greater chance of adsorbing, possibly through a rotationally trapped precursor. Clearly, orientational anisotropy plays a large role in determining the adsorption behavior for CO on Ni(111).

* Corresponding author. Fax: +1-650-725-0259.
E-mail address: zare@stanford.edu (R.N. Zare)
[1] Present address: Department of Chemistry, Wittenberg University, PO Box 720, Springfield, OH 45501, USA.

0039-6028/00/$ - see front matter
PII: S0039-6028(00)00481-7

Molecular nitrogen provides a useful complement to CO. Both molecules are isoelectronic and share the same mass, yet the sticking coefficient at 0.2 eV incident kinetic energies is 0.85 for CO–Ni(111) [3], whereas the sticking coefficient has been reported to be $<10^{-6}$ at room temperature for N_2–Ni(111) [4]. Interestingly, the bonding of N_2 to Ni(111) is similar to CO. N_2 bonds at the atop site, with its bond perpendicular to the plane of the surface [5]. CO bonds at an atop site or a bridge site, also with its bond along the surface normal [6]. Photoemission studies have shown that the N_2 molecular orbitals rehybridize near the surface and resemble those in CO. An excess of electron density in the $2p\sigma$ state resides on the N atom closest to the surface and is partially donated to the surface in the bonding interaction [7]. Yoshinobu et al. [5] have measured the heat of adsorption of N_2 on Ni(111) to be -8.4 kcal/mol. This value is roughly one-third of the bonding energy of CO on Ni(111), 30.5 kcal/mol [8]. Thus, despite the rearrangement of electron density, N_2 does not achieve the same strength of bonding as the very similar molecule CO does at an Ni(111) surface.

2. Experimental apparatus

The experimental apparatus has been previously described [9]. Briefly, a pulsed supersonic molecular beam impinges upon a single-crystal surface in an ultrahigh vacuum (UHV) chamber. The scattered molecules are state-selectively ionized and detected by time-of-flight (TOF) mass spectrometry.

2.1. REMPI/TOF detector

In order to state-selectively ionize the nitrogen molecules, we employ a spectroscopic detection scheme first utilized by Lykke and Kay [10] and subsequently studied in detail by Hanisco and Kummel [11]. This (2+1) resonance-enhanced multiphoton ionization (REMPI) transition involves the absorption of two photons of $\sim$202 nm to proceed from the vibrational ground state of the $X^1\Sigma_g^+$ electronic ground state to the ground vibrational state of the $a''^1\Sigma_g^+$ Rydberg electronic state. We use the Q-branch members of the (0, 0) band to determine the rotational populations because this branch is relatively insensitive to alignment effects. Tunable UV light for this transition is generated in the following manner. The second harmonic of a pulsed Nd:YAG laser (Continuum NY61-10) pumps a tunable dye laser (Lambda Physik ScanMate 2E) to produce light at about 606 nm. An angle-matched BBO crystal (Inrad Autotracker II) frequency doubles the dye laser output, and the residual dye fundamental and harmonic are mixed in a second angle-matched BBO crystal (Inrad Autotracker II). 60 mJ of dye laser output at 606 nm results in 12 mJ at 303 nm and 1 mJ at 202 nm. The 202 nm light is separated from the other wavelengths via five dichroic mirrors (Virgo Optics) and focused into the chamber with an uncoated 200 mm fused silica lens (CVI Optics). The final two dichroics are mounted on linear translation stages (Newport) that allow the laser focal volume to be accurately positioned in front of the surface.

After ionization, the scattered molecules are steered into a TOF tube and strike a 40 mm multichannel plate (MCP) array. The MCP signal is averaged in a digital oscilloscope (Tektronix TDS620) and acquired by a desktop computer for storage and analysis.

Experiments were done to determine the proper laser power normalization exponent. Hanisco and Kummel [11] found that an exponent of two was appropriate to fit their data, but at higher laser powers a value of 1.5 has been noted for (2+1) REMPI transitions corresponding to geometric saturation [12]. Indeed, we found that the appropriate exponent for our experimental conditions is 1.5. Once the peak heights for the various rotational states have been extracted, they are corrected for the nuclear spin statistics (g_J), rotational state degeneracy ($2J+1$), and the Bray–Hochstrasser two-photon line strength factors [13].

The resolution of the rotational spectra is so good that rotational states as low as $J=4$ are clearly resolved. In contrast, $J=0$ to 3 fall nearly on top of each other and cannot be resolved with this laser system. The method used to extract population information from the lowest rotational states is to assume that they are adequately

described by a single temperature. We fit the rotational populations of the state $J=4$ to $J=8$ to a temperature. Relative populations for that temperature are then calculated and assigned to the states $J=0$ to 3. We found a rotational temperature of 297 ± 4 K for a room temperature (298 K) sample of N_2. Therefore, we are confident that our laser and data collection and analysis system can give reliable and accurate quantum state distributions for a sample of nitrogen molecules.

2.2. Pulsed molecular beam

The molecular beam is comprised of a mixture of 5% N_2–95% He. The backing pressure on the nozzle (1 mm diameter) was optimized for the greatest rotational cooling as well as lowest velocity spread in the beam, and the optimal pressure was found to be 60 psi. In order to ensure that the molecular beam was rotationally cold, the rotational state distribution of the molecules in the incident beam was measured. Because the low rotational states of the Q branch lie nearly on top of one another for the (2+1) REMPI transition, the S-branch members are used to determine the relative populations of the rotational quantum states. The supersonic expansion from the nozzle is not expected to be in equilibrium, and, therefore, cannot be well-represented by a temperature. Nonetheless, a rotational temperature gives a good idea of the relative populations of the rotational quantum states, and the rotational temperature is less than 10 K determined by a fit to the three lowest rotational levels. Essentially, all of the molecules are in these lowest rotational levels. In addition, a measurement of the velocity spread of the beam indicates that the translational temperature was also approximately 10 K.

The pulse duration used for the angular distribution and rotational distribution was 300 μs in order to avoid any velocity-dependent effects on these distributions. For the surface position calibration, however, a chopper was introduced to decrease the pulse width to 15 μs.

2.3. The main (UHV) chamber

The UHV vacuum chamber is pumped by a liquid-nitrogen-trapped 10″ diffusion pump (Edwards E012) and achieves a base pressure of 5×10^{-10} Torr. Surface cleanliness and order are monitored using a reverse view LEED–Auger spectrometer (Fisons RVL 900), following sputtering with Ar^+ at 500 eV by an ion gun (Varian) and annealing for 30 min at 900 K. The sample is mounted on a three-axis manipulator with two independent angular rotations (Vacuum Generators). This manipulator provides for precise spatial positioning of the sample in the detector in three orthogonal directions. Additionally, the surface may be tilted $\pm70^\circ$ about an axis parallel to its face. A resistive heating filament behind the sample plate heats the sample to temperatures above 1100 K, as monitored by a chromel–alumel thermocouple spot-welded to the front face of the crystal. The thermocouple reading was checked against an optical pyrometer and found to be accurate to within 5 K.

2.4. Angular distribution determination

The angular distributions of N_2 scattered from the Ni(111) surface were collected for several incident angles and surface temperatures. The angular distributions were taken by placing the laser along an arc whose radius extends 2.0 cm from the intersection of the molecular beam and the surface. Because the intersection ellipse of the beam with the surface is approximately 1 mm in diameter and the laser focal point is less than 100 μm in diameter, the angular resolution of the technique is about 3–5°.

The laser must be placed at a constant distance from the surface because the intensity of the scattered molecules will decrease as the laser is moved further from the surface. A calibration of the location of the intersection of the beam with the surface is done to ensure that the laser is located at a reproducible position. The calibration is done by placing the surface so that the molecular beam is incident along the surface normal. The maximum of the scattered intensity will then be reflected back along the surface normal. The laser is then placed in front of the surface. By varying the time delay between the firing of the nozzle and the laser, a waveform of intensity at the laser focus versus time can be produced. Two peaks will be

seen that correspond to the incident beam and the scattered molecules. As the laser is moved closer to the surface, the two peaks will become closer because the incident beam will take longer to reach the laser, whereas the scattered molecules will take a shorter time. By changing the position of the laser along the surface normal, a graph of the laser position as a function of the time of maximum intensity for each peak can be generated. The slope of each line corresponds to the velocity of each peak. An example of this analysis is shown in Fig. 1. The intersection of the two lines corresponds to the location of the surface. This arrangement has been successfully utilized to measure the scattered velocities and angular distributions for other gas–surface systems, including N_2–Cu(110) [14,15], H_2–Cu(110) [16], and H_2–Pd(111) [17].

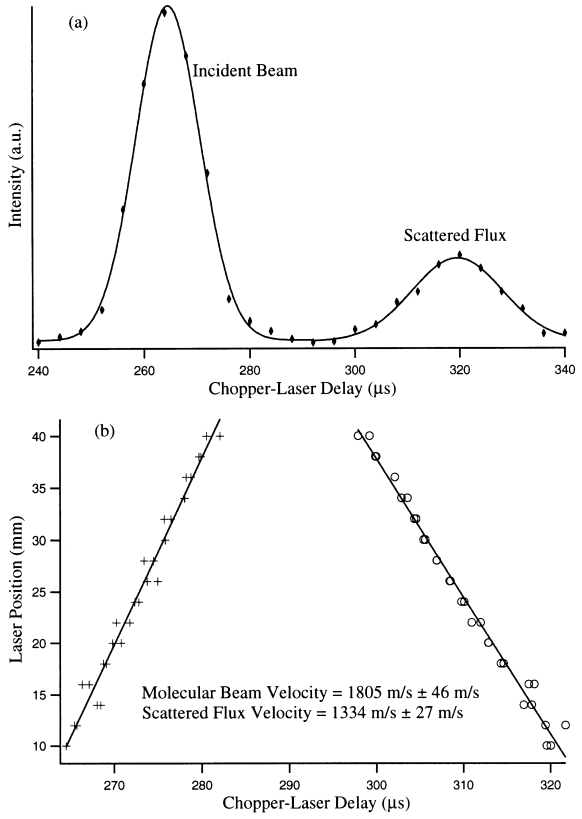

Fig. 1. Surface calibration procedure. (a) The ion signal produced by the passage of the molecular beam and the backscattered flux past the laser focal point. (b) The fit of the peak positions and the calculated velocity of the incident and scattered molecules. In this case, the scattered molecules ($J=8$) have only 55% of the initial translational energy.

3. Results

3.1. Rotational energy distributions

The rotational energy distributions of molecules scattered from the Ni(111) surface were collected at surface temperatures of 303, 573, and 873 K at incident angles θ_i varying from 15 to 60° from the surface normal. The spectra taken near the specular direction show substantial deviations from Boltzmann distributions, although no rotational rainbows are observed. Fig. 2 shows rotational distributions for molecules that leave the surface near the specular angle (Fig. 2a). In contrast, molecules that leave the surface in a direction far from specular tend to have distributions that more closely resemble Boltzmann distributions. Such distributions are shown in Figs. 2b and 3. Fig. 2b shows a distribution taken at the far superspecular, and Fig. 3 shows a distribution taken to the far subspecular.

Because the distributions were often non-Boltzmann, we have chosen to compare the amounts of rotational excitation of the scattered molecules by computing a mean rotational energy per molecule for each distribution. Although this method of quantifying the distribution can be prone to errors due to noise in the high-J populations, this method is superior to using rotational temperatures that do not accurately describe the distributions. One potential source of systematic error in these measurements is the failure to capture the entire distribution, which would tend to lower the observed mean rotational energy. In order to avoid this issue, the laser scan was made over a sufficient range such that a clear baseline was established. The amount of noise caused by omitting several high-J peaks was found to be on the order of 25 cm^{-1}. In Fig. 4, these values are plotted as a function of exit angle θ_f from the surface normal for each of the incident angles and surface temperatures. The horizontal lines correspond to the energy that would be expected for molecules that have equilibrated completely with

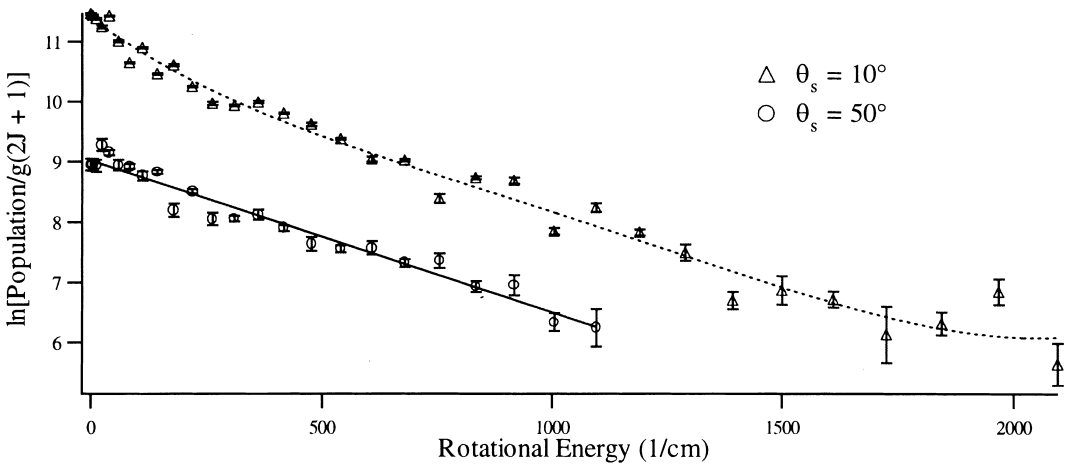

Fig. 2. Rotational distributions for (a) $\theta_i = -15°$, $\theta_f = 10°$ and (b) $\theta_i = -15°$, $\theta_f = 50°$. Distribution (a) taken near the specular direction is clearly non-Boltzmann. Distribution (b) taken at the far superspecular fits more closely to a Boltzmann distribution. The dashed line is a fit of $J=0$ to $J=22$ to a Boltzmann distribution at 438 ± 15 K, and the mean rotational energy of distribution (a) is $334 \pm 15\ cm^{-1}$. The solid line is a fit of $J=0$ to $J=23$ to a Boltzmann distribution at 571 ± 23 K, and the mean rotational energy of distribution (b) is $318 \pm 26\ cm^{-1}$. The surface temperature is 573 K.

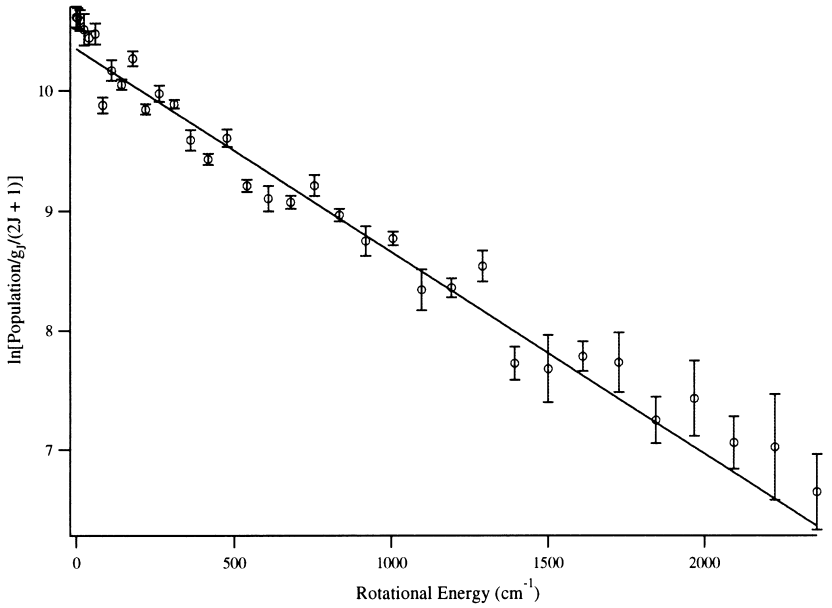

Fig. 3. Rotational distribution for $\theta_i = -60°$, $\theta_f = -50°$ This distribution is taken to the far subspecular, and the line is a fit to a Boltzmann distribution with a rotational temperature of 852 ± 16 K. The surface temperature is 873 K. The mean rotational energy is $568 \pm 21\ cm^{-1}$.

the surface, whereas the vertical lines correspond to the specular angle. In general, the graphs show that molecules that leave the surface close to the specular direction tend to have mean rotational energies that are independent of the surface temperature. In addition, the value of the mean rotational energy near the specular direction for all incident angles is approximately $330\ cm^{-1}$, which

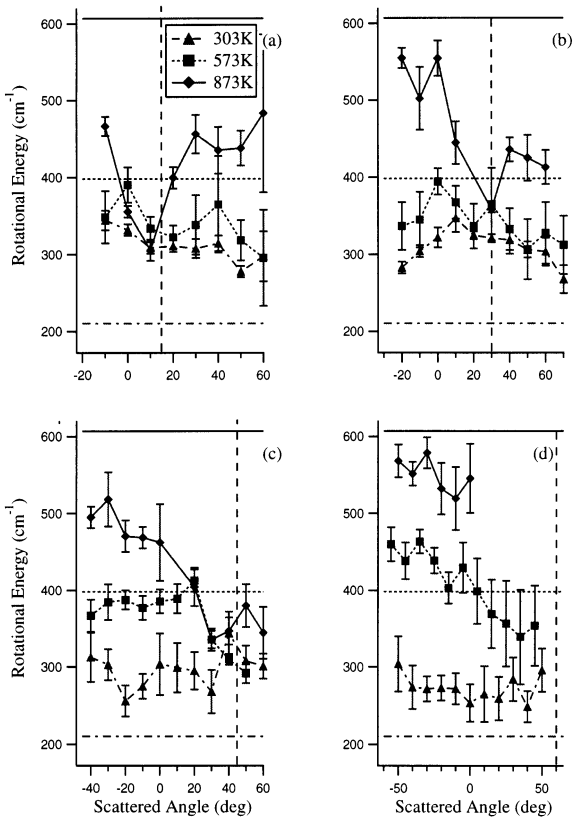

Fig. 4. Mean rotational energies as a function of scattering angle for several incident angles and surface temperatures. The horizontal dashed–dotted line corresponds to $T_s = 303$ K, the dotted line to $T_s = 573$ K, and the solid line to $T_s = 873$ K. The incident angles are (a) $\theta_i = -15°$, (b) $\theta_i = -30°$, (c) $\theta_i = -45°$ and (d) $\theta_i = -60°$. The error bars correspond to the propagation of error from uncertainties in the height of the ion signal peaks in the power normalized spectra.

corresponds to 10% of the translational energy of the incoming nitrogen molecules. Molecules that leave that surface in a direction far from specular exhibit mean rotational energies that vary with the surface temperature.

3.2. Angular distributions

The angular distributions of N_2 scattered from the Ni(111) surface have been collected for several incident angles and surface temperatures. In general, for a given angle of incidence, we observe scattered molecules for a broad range of exit angles. By comparing the scattered ion intensity with the one from background N_2 gas, the angle-dependent detection efficiency was determined and a quantitative evaluation was performed.

The angular distributions show a distinct dependence on surface temperature and on angle of incidence. In Fig. 5, angular distributions for $J = 4$ and $J = 24$ are shown for angles of incidence of $\theta_i = -15°$ and $\theta_i = -45°$. For θ_i up to $-45°$, a prominent specular reflection is seen for the two high temperatures. Scattering from a room-temperature surface reveals a nearly structureless distribution. In addition, the specular seems to be less pronounced or absent for high-J states.

4. Discussion

Because the sticking coefficient of N_2 on Ni(111) at room temperature is negligible [4], we expect to see little evidence for trapping of N_2 at the surface temperatures used in this study. We interpret our results to show that the molecules do not trap, but a significant fraction of the molecules do experience several collisions with the surface before leaving the surface. The rotational distributions appear to support this hypothesis. During the course of a collision with the surface, the molecule must lose enough translational energy to the surface or to other internal energy modes in order to trap. If this loss does not occur, the molecule leaves after bouncing from the surface, and there is little opportunity for the surface to exchange energy with the molecule. The rotational distributions should then be expected to show little dependence on the surface temperature. This behavior occurs near the specular direction for the molecules that are incident at 15, 30, and 45°. A similar independence on surface temperature has been observed in the rotational distributions of N_2 scattered from W(110) and Pt(111) [18], in the alignment of N_2 scattered from Ag(111) [19], and in the scattered rotational distributions of CO from Ni(111) [2].

Molecules that fail to escape the potential energy well after the first bounce will suffer another collision with the surface. With each additional collision, these molecules will become more equili-

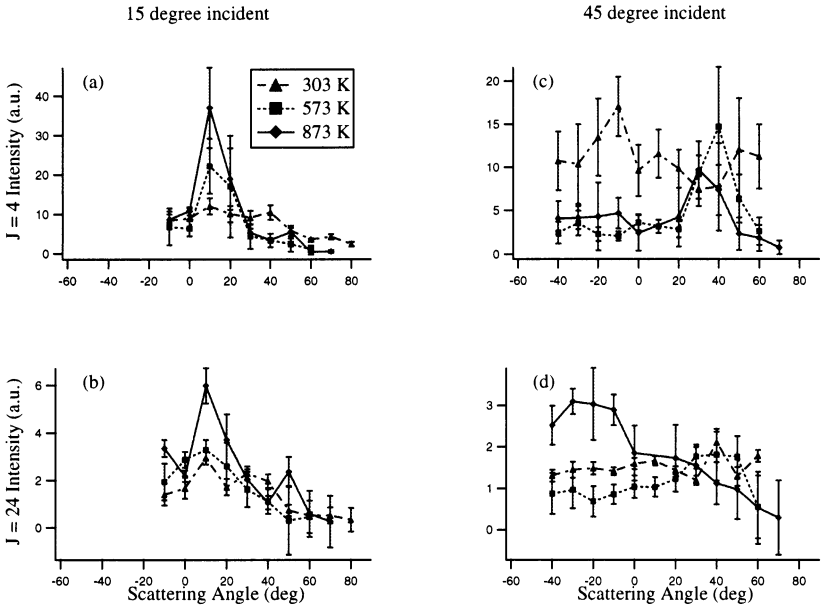

Fig. 5. Angular distributions for the N_2–Ni(111) system. The dashed–dotted lines correspond to 303 K, the dotted lines to 573 K, and the solid lines to 873 K. The incident angle and rotational level for each plot are (a) $\theta_i = -15°$, $J=4$; (b) $\theta_i = -15°$, $J=24$; (c) $\theta_i = -45°$, $J=4$; and (d) $\theta_i = -45°$, $J=24$.

brated with the surface. The angular distributions of these molecules will also be broader than that of the molecules undergoing single-bounce trajectories because they will have a greater chance of losing 'memory' of their initial momenta. This behavior is quite apparent in the rotational distributions of N_2 incident at 60°. The degree of accommodation with the surface is not complete, but a significant dependence on the surface temperature is observed. Siders and Sitz [15] interpret their high-temperature rotational rainbows as evidence for multiple bounces in the N_2–Cu(110) system for similar incident energies, and the well depth for this system is 0.10 eV, which is less than half of the well depth for N_2–Ni(111). Thus, the N_2–Ni(111) system should also be expected to exhibit multiple-bounce trajectories.

The angular distributions presented in Fig. 5 also show evidence for multiple-bounce trajectories. The near-specular peak is most obvious in the distributions corresponding to low-J states. These molecules convert a relatively small amount of translational energy into rotation and, therefore, can more readily leave the potential well. In the absence of corrugation, the scattering angle is dependent on the amount of perpendicular momentum that is transferred to the surface, as well as on the degree of rotational excitation. The near-specular peak becomes broader as the incident angle is increased. This trend may be caused by the increased importance of multiple-bounce trajectories. Because molecules incident at 45° have only 50% of the initial momentum directed perpendicular to the surface, they are more likely to remain on the surface after the first bounce.

Similarly, molecules that scatter into high-J states have substantially broader angular distributions. At an incident angle of 45°, the high-J distribution shows no specular peak. The absence of a clear specular peak is indicative of an interaction with the surface that is dominated by multiple bounces. Since the equilibrium geometry of the bound N_2 is on the atop site with its bond axis perpendicular to the surface, molecules that arrive at the surface side-on will experience a torque to bring the molecule to a perpendicular geometry. In contrast, molecules that arrive at the surface end-on should experience significantly less

torque and will be less rotationally excited. Although the degree of rotational anisotropy in the potential for this system is unknown, the deepest part of the potential well should correspond to the equilibrium geometry, and molecules that do not approach the surface in the optimal geometry should be steered towards this geometry. These highly rotationally excited molecules will have less translational energy available to escape. They will require two or more collisions with the surface in order to gain sufficient translational energy to escape.

The behavior of N_2 scattered from Ni(111) is quite different than that of CO scattered from the same surface. Rotational rainbows are noticeably absent in the scattering of N_2. A rotational rainbow is a local maximum in the rotational energy level population distribution [20]. Hines and Zare [2] observed rotational rainbows in the scattering of CO from Ni(111), and they attributed the rainbow to scattering from the O-end of the CO molecule. Because the O-end of CO interacts very weakly with Ni(111), the weak interaction of N_2 with Ni(111) might be expected to cause rotational rainbows in the scattering of N_2 from Ni(111). In addition, Sitz et al. [19] observed rotational rainbows in the scattering of N_2 from Ag(111). One possible explanation for the absence of such rotational rainbows is the surface temperature: the high surface temperature results in a large displacement of the surface atoms away from their equilibrium positions. The temperatures used in this study are significantly higher than those used in the N_2–Ag(111) study (90 K). At any given instant in time, then, the surface appears rough. A more corrugated surface and the averaging over impacts with surface atoms of varying velocities could wash out the rotational rainbow in comparison with a smoother surface.

Another possibility for the absence of rotational rainbows is the relative size of the N_2 potential energy well compared with the incident kinetic energy. Because the incident kinetic energy used in this experiment is only slightly larger than the well depth determined by Yoshinobu et al. [5], it is likely that molecules that are highly rotationally excited are preferentially trapped by the surface because most of the energy used in the rotational excitation originates in the initial translational energy. This preferential trapping appears in the 45° angular distributions. A similar case occurs for CO–Ni(111). Because CO is a heteronuclear diatomic molecule, two rotational rainbows would be expected, but a rainbow corresponding to 'C-end' collisions is not seen. The reason for this behavior, as proposed by Hines and Zare [2], is that CO molecules that scatter into the C-end rainbow are trapped by the deep attractive well. A rainbow was observed to occur at $J=20$ for CO–Ni(111) [2] and at $J=17$ for N_2–Ag(111) [19] at similar incident energies to our work. We see no evidence of rotational rainbows at levels up to $J=30$. Because the position of the rainbow is related to the depth of the potential energy well, the N_2–Ni(111) well depth should be considerably larger than that for N_2–Ag(111), about 0.1 eV, or for the 'O-end' well of the CO–Ni(111) system.

5. Conclusions

The scattering of N_2 from Ni(111) results in the conversion of about 10% of the translational energy into rotational excitation. The degree of rotational excitation is found to be independent of the surface temperature for scattering near the specular direction, but it is dependent on the surface temperature at scattering angles far from the specular direction. We do not observe rotational rainbows in the scattered rotational distributions under any of the conditions studied. The angular distributions show that the molecules leave the surface in a broad distribution that is dependent on the degree of rotational excitation and the incident angle and indicate that the interaction between N_2 and Ni(111) appears to be sufficiently strong to allow multiple-bounce scattering trajectories. This interaction, however, does not allow for trapping under the conditions used in this study.

Acknowledgements

The authors acknowledge financial support from the National Science Foundation (Grant No.

CHE-9900305). One of the authors (C.M.M.) acknowledges support from the Hertz Foundation, and F.B. acknowledges the Deutsche Forschungsgemeinschaft (Ba 1858/1-1 and Ba 1858/1-2).

References

[1] J.A. Barker, D.J. Auerbach, Surf. Sci. Rep. 4 (1984) 1.
[2] M.A. Hines, R.N. Zare, J. Chem. Phys. 98 (1993) 9134.
[3] S.L. Tang, J.D. Beckerle, M.B. Lee, S.T. Ceyer, J. Chem. Phys. 84 (1986) 6488.
[4] V. Zhukov, A. Ferstl, K. Rendulic, Fizika A 4 (1995) 271.
[5] J. Yoshinobu, R. Zenobi, J. Xu, Z. Xu, J.T. Yates Jr,, J. Chem. Phys. 95 (1991) 9393.
[6] S.L. Tang, M.B. Lee, Q.Y. Yang, J.D. Beckerle, S.T. Ceyer, J. Chem. Phys. 84 (1986) 1876.
[7] K. Horn, J. DiNardo, W. Eberhardt, H.-J. Freund, E.W. Plummer, Surf. Sci. 118 (1982) 465.
[8] J.B. Miller, H.R. Siddiqui, S.M. Gates, J.N. Russell Jr,, J.T. Yates Jr,, J.C. Tully, M.J. Cardillo, J. Chem. Phys. 87 (1987) 6725.
[9] M.D. Ellison, C.M. Matthews, R.N. Zare, J. Chem. Phys. 112 (2000) 1975.
[10] K.R. Lykke, B.D. Kay, J. Chem. Phys. 95 (1991) 2252.
[11] T.F. Hanisco, A.C. Kummel, J. Phys. Chem. 95 (1991) 8565.
[12] D. Zakheim, P. Johnson, Chem. Phys. 46 (1980) 263.
[13] R.G. Bray, R.M. Hochstrasser, Mol. Phys. 31 (1976) 1199.
[14] J.L.W. Siders, G.O. Sitz, J. Chem. Phys. 101 (1994) 6264.
[15] J.L.W. Siders, G.O. Sitz, J. Vac. Sci. Technol. A: 13 (1995) 1400.
[16] M. Gostein, H. Parhikhteh, G.O. Sitz, Phys. Rev. Lett. 75 (1995) 342.
[17] M. Gostein, E. Watts, G.O. Sitz, Phys. Rev. Lett. 79 (1997) 2891.
[18] T.F. Hanisco, A.C. Kummel, J. Chem. Phys. 99 (1993) 7076.
[19] G.O. Sitz, A.C. Kummel, R.N. Zare, J. Chem. Phys. 89 (1988) 2558.
[20] A.W. Kleyn, A.C. Luntz, D.J. Auerbach, Surf. Sci. 117 (1982) 33.